Scientific report; WR 94-04

Ministerie van Verkeer en Waterstaat
Koninklijk Nederlands
Meteorologisch Instituut

Cloud-Radiation-Hydrological interactions: Measuring and Modeling

A.J. Feijt
R. van Dorland
A.C.A.P. van Lammeren
E. van Meijgaard
P. Stammes

KNMI

De Bilt, 1994

Scientific report; WR 94-04

De Bilt, 1994

Postbus 201
3730 AE De Bilt
Wilhelminalaan 10
Telefoon 030-206 911
Telefax 030-210 407

UDC: 551.501.721
551.501.776
551.506.24
551.521
551.576.11
551.579
551.583
ISBN: 90-369-2062-0
ISSN: 0169-1708

Clouds–Radiation–Hydrological interactions

Measuring and Modeling

A.J. Feijt
R. van Dorland
A.C.A.P. van Lammeren
E. van Meijgaard
P. Stammes

This report describes the project: 'Clouds–Radiation–Hydrologic interactions in a limited area model'. The project was carried out in the framework of the Dutch National Research Program on Global Air Pollution and Climate Change (NOP) and supported by NOP under contract number 8520587.

Summary

The KNMI has built an environment to study clouds–radiation–hydrologic interactions for climate model development. A cloud detection system which provides high resolution cloud characteristics over an area of 100*100 km^2 has been installed. Cloud fields were studied to assess the merits of the system. Observations will be used to validate parametrization schemes of clouds and radiation in climate models. Global data sets on clouds and radiation were evaluated for use in climate modeling. An environment for climate model development has been built. The climate model radiative transfer scheme has been improved with respect to atmospheric constituents which dominate the enhanced greenhouse effect. A line–by–line model has been developed to study radiative transfer with high spectral resolution.

LIST OF CONTENTS

1. INTRODUCTION

Clouds play an important role in our climate. Clouds produce precipitation which is an essential ingredient of the hydrological cycle. Clouds modify the earth–radiation budget. Thin cirrus clouds have a warming effect while low clouds have a distinct cooling effect (Ramanathan, 1989). Clouds dominate the vertical transport of energy, momentum and trace gasses in the free troposphere

Despite their importance, clouds are represented only rudimentary in climate and weather forecast models. It appears that the model representation of clouds in climate models has a major impact on model predictions for climate change. Cess et al. (1989) showed that cloud feed–back is a major source of uncertainty in model responses to climate forcing.

There are two main reasons why the uncertainties with respect to clouds are so large. The first reason is that cloud processes are extremely complicated. A proper representation of clouds requires the parameterization of processes both on the macro–scale (cm – km) and on the microscale (<<cm).

The second reason is the lack of good quantitative observations of cloud characteristics (cloud cover, cloud structure, optical depth, droplet spectra). High resolution measurements are crucial for the development and improvement of parameterization schemes for clouds and cloud–radiation interactions.

Satellites begin to provide useful data on global cloud statistics and corresponding radiation budgets. The International Satellite Cloud Climatology Project (ISCCP) data set contains information on global distribution of clouds, their height, temperature, optical thickness, etc. The Earth Radiation Budget Experiment (ERBE) data set contains information about the global distribution of shortwave and longwave radiation at the top of the atmosphere. Both global data sets are derived from satellite measurements. They improve the understanding of cloud related processes. Despite their usefulness the global data sets on clouds and radiation are not fully validated. To validate these global data sets on a regional scale, detailed measurements of the cloud cover and structure are necessary. It is important to measure the variability of the cloud characteristics and to study in detail the basic assumptions of the processing schemes.

The aim of the project "Clouds–Radiation–Hydrologic interactions in a limited–area model" is threefold:

1) Provide a detailed regional data set on cloud cover and cloud characteristics.
2) Analyse the ISCCP and ERBE data sets with respect to validity and possible applications for climate model verification.
3) Create a model environment for the enhancement of regional data analysis and for the improvement of parameterizations of clouds and radiation.

In this report an overview is given of the activities for this project. A description of the KNMI Cloud Detection System (CDS) is given by Arnout Feijt and André van Lammeren in section 2,

followed by a case study of the merits of the CDS in section 3.

Analysis of the ISCCP and ERBE data sets is described by Arnout Feijt in sections 4 and 5. The ISCCP cloud detection algorithm is evaluated, some initial results on global cloud amount are presented. The ERBE data processing scheme is studied. The reliability of ERBE data for climate research purposes is evaluated.

Model development is described in section 6. Erik van Meijgaard constructed and implemented the Regional Atmospheric Climate Model (RACMO), which is used to study in detail the local implications of global climate change. A flexible model development environment was built.

Rob van Dorland studied the atmospheric radiative transfer parametrizations for climate modeling purposes. He improved the representation of trace gasses, ozone and aerosols for application in the Hamburg climate model. The radiation schemes are described in section 7.

Piet Stammes developed a line–by–line radiative transfer model, which is suitable for validation of the climate model radiation schemes. The method and some computational results are presented in section 8.

Detailed descriptions of the parts of this project are reported to the scientific community through papers and contributions to conferences.

2. THE KNMI CLOUD DETECTION SYSTEM

INTRODUCTION

A proper description of clouds and cloud–radiation interactions in climate models requires the parametrization of processes which determine cloud cover and cloud structure within one model gridbox. To validate and improve these parametrizations a set of measurements is required. A Cloud Detection System (CDS) is developed which yields accurate and high resolution cloud measurements over the Netherlands for a period of at least two years. In this system both ground based and satellite remote sensing instruments data are combined. The CDS is used to retrieve the information on the 3– dimensional structure of cloud ensembles.
A description in full detail is given by Stammes et al. (1994). An outline is given below. The performance of the CDS is illustrated with a case study. The CDS is operational since October 1994.

INSTRUMENTATION

The cloud detection system consists of a network of stations for ground based remote sensing and a processing and archiving environment for NOAA/AVHRR and Meteosat measurements. At two sites extensive radiation measurements are done to obtain data for the analysis of cloud–radiation interactions.

Ground based measurements

The network stations are located in a 120*120 km^2 area in the Netherlands (fig.1). The area is characterized by a moderate marine climate with a prevailing westerly circulation. Each ground station consists of:

* lidar ceilometer
  wavelength: 908nm
  frequency: 1 measurement per minute
* narrowband infrared radiometer
  FOV = 50 mrad,
  wavelength: 9.6–11.5 μm,
  frequency: 1 measurement per second
* pyranometer
  wavelength: 0.3 – 3.0 μm

More extensive ground measurements are performed at the meteorological tower at Cabauw, which is located near the center of the area. Up to 200m the mean vertical profiles are measured of temperature, humidity, visibility and wind speed and

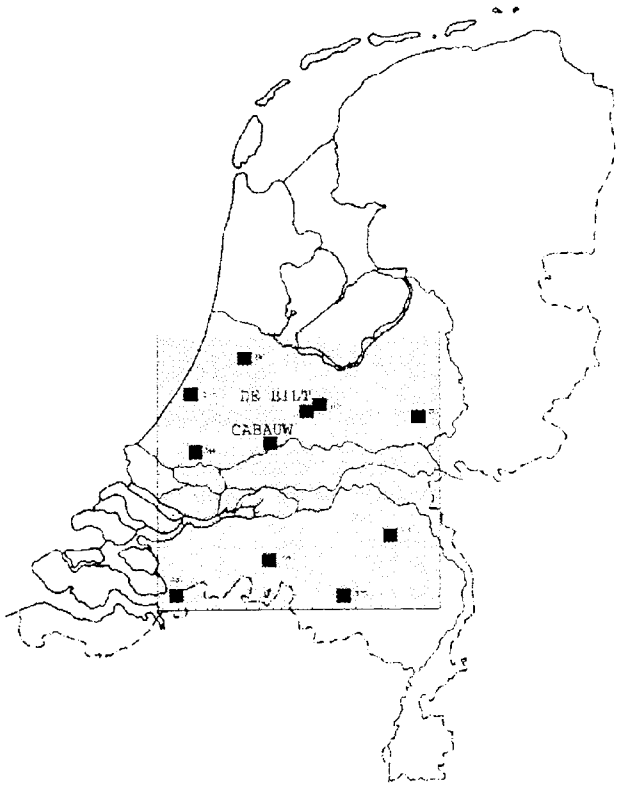

fig. 1: Network stations of the KNMI cloud detection system

direction. A wind profiler with a Radio Acoustic Sounding System (RASS) is available for measurements of horizontal and vertical windspeed, and temperature with a high temporal and vertical resolution in the boundary layer (Monna, 1994). Also a video–camera (color S–VHS system) is installed, which takes an image of the sky each 3.2s. The recordings are an invaluable aid in interpreting the other measurements.

Radiation measurements

Extensive radiation measurements are done over grassland and Douglas forest respectively. This provides data for the analysis of cloud–radiation interactions. Measured radiation budget components are: longwave down– and upwelling radiation and shortwave global, diffuse and direct radiation.

Satellites

The AVHRR instruments orbit on the NOAA polar sun–synchronous satellites at 850 km altitude. The Instrument consists of 5 narrow band channels at 0.63, 0.83, 3.7, 11.8 and 12.0 μm respectively. The sub–satellite resolution, the footprint, is 1.2 km. Each NOAA satellite passes over the Netherlands two times per day. There is a morning and an afternoon satellite, so there are 4 AVHRR measurements per day. At the KNMI AVHRR data are received and processed real–time.

The AVHRR Processing scheme Over cLouds, Land and Ocean (APOLLO) (Saunders et al. 1986, 1988) is used for detection of cloud contamination and fully cloudy pixels from AVHRR measurements. Cloud properties which are retrieved using APOLLO extensions are: cloud cover fraction, cloud top temperature (Saunders, 1988), reflectivity, optical thickness (Kriebel, 1989), ir– emissivity and ice–detection (Gesell, 1989). The SHARK–APOLLO satellite data analysis package (Gesell, 1993) will be used for routine analysis. Local implementations of the retrieval methods of cloud properties will be used for evaluation, validation and development purposes.

The Meteosat satellites are geo–stationary at about 0° latitude and 0° longitude. The instrument consists of three broadband channels for detection of:

* reflection of visible (solar) radiation (0.4–1.1 μm)
* water vapor absorption (5.7 – 7.1 μm)
* thermal infrared radiation (10.5 – 12.5 μm)

The sub–satellite resolution is 5x5 km^2. At our latitude the resolution is degraded to 5x9 km^2. Images are available every half hour.

At the KNMI an algorithm inspired on the the ISCCP–cloud detection scheme (Rossow, 1993) is under development to analyze the Meteosat measurements (Feijt et al., 1994).

Weather forecast analysis data on air temperature is used to perform dynamic thresholding of the infrared tests.

Auxiliary data

Information on the actual atmospheric conditions is available for the interpretation of the

measurements. The HIgh Resolution Limited Area Model (HIRLAM), operational at KNMI, and RACMO will provide information on temperature and humidity profiles, and wind speed and direction on a 50km scale. The 6-hourly rawinsonde data from de Bilt, close to the center of the TEBEX area, are available.

Precipitation is detected at each CDS ground station and by operational weather radars. The amount of precipitation is measured at each CDS ground station using a rain gauge.

Radiative transfer calculations for atmospheric correction of longwave radiation are performed using Lowtran-7 (Kneizys et al., 1988).

MEASUREMENTS AND PRODUCTS

Archive

The aim is to obtain continuous data on clouds and radiation for a period of two years.For satellite instruments data will be archived for a larger area. This makes it possible to examine the mesoscale atmospheric processes in which the small-scale processes are embedded.

The following data will be archived:

a) Satellite instruments

instrument:	NOAA – AVHRR	Meteosat
area:	350*550 km2	1500*1000 km2
data archived:	radiances all 5 channels.	radiances all 3 channels
frequency:	4 times a day. Each half hour	

b) Ground based instruments

instrument:	lidar (ceilometer)	infrared radiometer
spectral range:	904-911nm	9.6-11.5 micron
data archived:	backscatter profile every 60s	10-minute characteristics of zenith radiances
limitation:	maximum height 4km	minimum temperature -50 ^{0}C

In addition we archive the 3-hourly HIRLAM analyses for an area of 1500*2000 km^2 in North-west Europe, and the 6-hourly de Bilt rawinsonde

Products

The cloud detection system is used to retrieve the distribution of the following cloud characteristics:

* cloud cover
* cloud top temperature
* cloud base height
* cloud base temperature
* cloud size

* reflectivity
* optical thickness
* liquid water content.

3. CASE STUDY: August 4, 1993

INTRODUCTION

On the 4th of August 1993 there was a high pressure system over Eastern Europe and a low pressure system over Norway (fig. 2). A weak cold front moved slowly over the Netherlands to the West. Surface pressure at the front was relatively high, 1020 hP. At noon the radiosonde shows an inversion at 3 km, −1 °C, indicating a small chance on showers. After the passage of the front there is backing wind with height indicating cold advection. At 3 km height the wind direction is South–West –South, at 13 m/s. At the surface the windspeed was about 4 m/s.

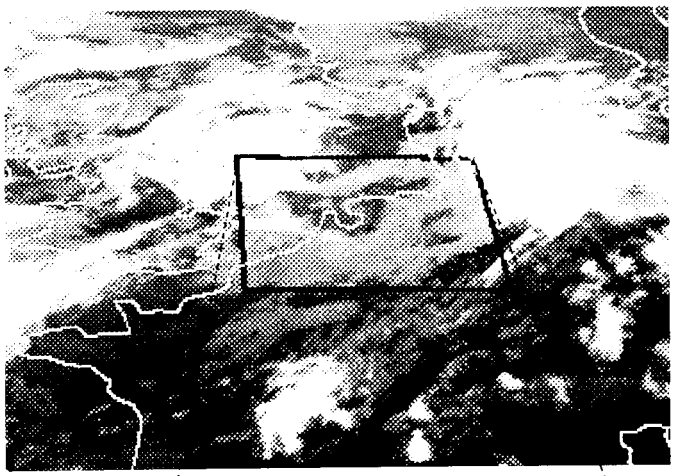

fig. 2: Meteosat infrared image at 7:30 UTC. Scaling: black T > +15C; white T < −15C...

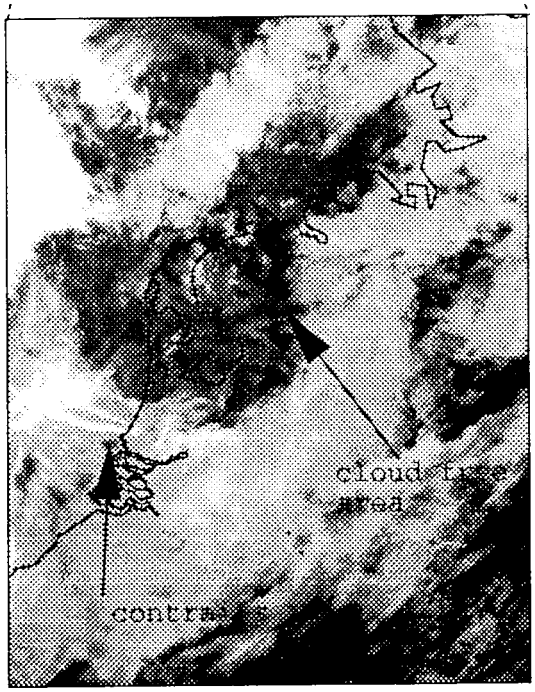

fig. 3: AVHRR image (channel 4) at 7:20 UTC. Scaling as in fig. 2.

Available data

The data from 6 until 12 UTC are studied in detail. The following data was available for analysis:

Satellite data

* Meteosat data every 30 minutes
* NOAA – AVHRR passage at 7:20 UTC

Ground based measurements

At De Bilt and Cabauw

* continuous Lidar measurements

At Cabauw only

* IR radiometer measurements
* continuous radiation budget measurements
* continuous video recording

Other data

* HIRLAM analysis data at 6, 9 and 12 UTC
* rawinsonde at 6 and 12 UTC at De Bilt

Data from the special lidar system of the network station in De Bilt at the National Institute of Public Health and Environmental Protection (RIVM) was used. This Lidar is more powerful and has a better S/N ratio compared to the Lidar ceilometers.

Analysis of satellite observations

On the Meteosat infrared image of 7:30 UTC two regimes can be identified (fig. 2). In the South there are convective clouds in a further

cloud free environment, which indicates a high pressure zone. In the North there is a variety of cloud ensembles, indicating low pressure areas. There is a band of mid–level clouds over the Netherlands. Closer examination of this cloud layer is possible with the AVHRR images of 7:20 UTC. Channel 4 shows the frontal cloud band in more detail (fig. 3). Also we identify streaky patterns which indicate contrails. The contrails are generated by airplanes which visit Amsterdam airport.

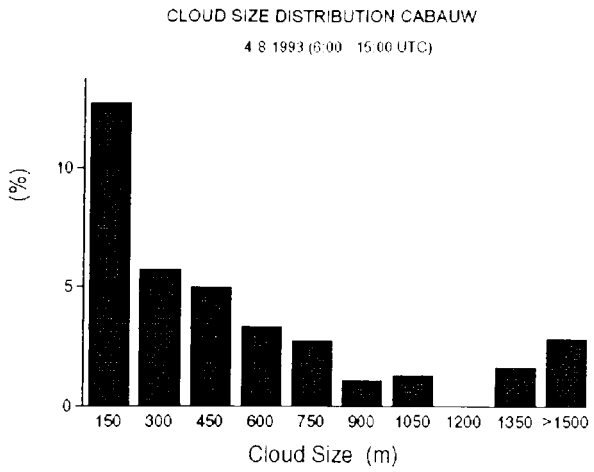

fig. 4: The measured cloud size distribution for the lower cloud layer in Cabauw between 6 – 15 UTC.

When running the APOLLO scheme, the scheme labels nearly all pixels as cloud contaminated. Only in the South– East there is an area, which is labeled cloud free. The frontal cloud band is labeled as fully cloudy.Channel 4 radiances were corrected for atmospheric influences using Lowtran–7 and the radiosonde profile of 6 UTC. According to the AVHRR, channel 4 calculations the fully cloudy pixels indicate cloud top temperatures of 0 to 5^{0}C.

Reflectivity of the whole system of atmosphere, cloud layer and surface, of the fully cloudy pixels, according to pre–flight calibration and assuming isotropic reflection, varies between 40 and 80%. From a cloud free area we measure he reflectivity of the atmosphere + ground system to be 8%.

Analysis of ground based observations

From the Lidar measurements we can conclude that between 6 and 12 UTC there are at least two cloud layers. One at approximately 2.7km and one at 0.5km. The lower layer could not be identified from satellite. The cloud fraction is estimated from time series. The time fraction that a cloud in the height range of the cloud layer is detected equals the cloud fraction, if a homogeneous spatial distribution of clouds (no cloud bands) is assumed. The mean cloud fraction of the lower cloud layer at Cabauw was 35%, for the time period from 6 to 15 UTC.

From the lidar measurements an estimate of the cloud size distribution is made. If two consequetive measurements of cloud base height do not differ more than a specified threshold, they are thought to originate from the same cloud. The product of the time that the cloud is detected and the wind speed at the cloud base yields the cloud size. Figure 4 shows the cloud size distribution at Cabauw for the lower cloud layer from 6 to 15 UTC. The distribution is dominated by small (< 150 m) clouds. Between 150 m and 1 km the frequency of occurrence decreases. For larger clouds the distribution is random due to the small number of occurrence.

Windward of the Cabauw lidar the reflectivity of the cloud field ranges from 40–50%. Preliminary radiative transfer calculations using the DAK model indicate that 40% reflectivity in this viewing geometry corresponds to an optical depth in the order of 8. The methods by Stephens (1978) and

Rossow (1988) yield comparable results.

From the infrared radiometer data we can identify both cloud layers. The lower layer has a cloud base temperature of about 10^0C, while the higher layer has a base temperature of about 0^0C. These temperatures were corrected for the atmospheric constituents using Lowtran–7 and radiosonde data. Comparison of the lidar cloud base height and radiometer cloud base temperature with the radiosonde temperature and dew–point temperature show good agreement (fig. 6). The total cloud cover over the frontal cloud band (low or high cloud) is close to unity according to both satellite and ground based instruments.

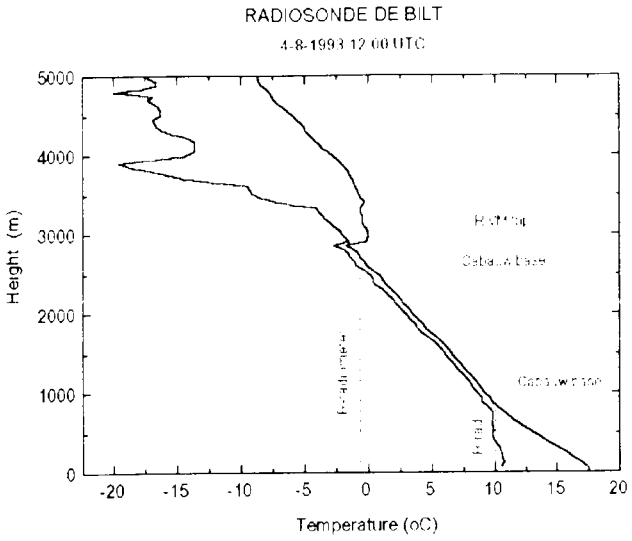

fig. 5: The rawinsonde temperature (solid) and dewpoint temperature (dashed) profiles from 6 UTC

CONCLUDING REMARKS

Data from the KNMI cloud observational network was analyzed for 4 August 1993. Although only one station for ground based remote sensing was available these measurements contributed largely to the understanding and characterization of the observed cloud field. Infrared measurements from the ground are consistent with AVHRR and Meteosat measurements, characterizing a relatively uniform cloud layer at 2.7km. Ground based lidar measurements revealed a second lower cloud layer, which is invisible to the satellite. A cloud size distribution is derived for this cloud field. For the characterization of the cloud field within the target area however, we need more information on the spatial and temporal variability. A first attempt has been made on the characterization of the cloud field mean optical depth from satellite.

ACKNOWLEDGMENTS

The authors want to thank Dr. E.P. Visser of the National Institute of Public Health and Environmental Protection (RIVM) for the use of the RIVM–lidar in the network. We would also like to thank Dr. P. Stammes for calculation of the cloud optical depth from satellite radiances.

4. ISCCP

AIM

The aim of our study is to evaluate the ISCCP data set for use in climate modeling. We evaluate the cloud detection algorithm, obtain insight into error–sources and errors in the derived cloud amounts and cloud properties on a global and regional scale.

INTRODUCTION

The International Satellite Cloud Climatology Project was first proposed at the Joint Organizing Committee (JOC) study conference on the parametrization of clouds and radiation for climate models (WMO, 1978). The concept which evolved from the proposal is to utilize observations from operational meteorological satellites to derive a global cloud climatology. The data set should support three kinds of activities:

* Data analysis: Development of climate indices and correlations with other climate data.
* Model validation: Improvement of cloud radiative models and models of the hydrological cycle, leading to improved understanding of the physical conditions under which clouds form and dissipate, and their relationship to precipitation and evaporation.
* Sensitivity studies: Understanding the extent to which clouds serve as tracers of weather and climate and the reverse, the impact of clouds on weather and climate.

The ISCCP archives satellite data since 1 July 1983 (WMO, 1982, 1986).

The ISCCP C1 products are processed globally each 3 hours at 280 km resolution (Rossow et al., 1991). For each grid cell cloud characteristics are derived: Cloud amount, cloud top pressure, cloud optical thickness and the spatial variations in these quantities. Averaged surface properties: pressure, temperature and visible reflectance are given. Average radiances for clear and clouded areas are given.
The C2 data contain monthly averages per grid cell. Cloud top pressure, top temperature and optical thickness are derived for 10 synoptical cloud types.

Nowadays, the ISCCP products are actually used in climate research. The cloud climatology is used by climate modelers to check if their General Circulation Models (GCM) obtain a trustworthy distribution of cloud amounts over the globe. Instantaneous measurements are used in combination with collocated ERBE measurements to calculate the global impact of clouds on radiation (Ramanathan, 1989), the so–called cloud radiative forcing.

In the following paragraphs the ISCCP cloud detection algorithm will be outlined and evaluated.

THE CLOUD DETECTION ALGORITHM

In the following we will evaluate the cloud detection algorithm, because it is the basis to all other products. To evaluate the algorithm two complimentary approaches are used. The first approach gives insight into the relationship between meteorological phenomena, remote sensing and the algorithm. Implicit in the algorithm are assumptions about the climate: the rate with

which surface temperature can change in space and time. These assumptions are studied using knowledge of meteorological phenomena and a local implementation of the first steps of the algorithm for North–West Europe below 55 degrees North. The literature on the ISCCP data set in comparison with other data sets is studied to obtain error statistics. In the next paragraph an outline of the algorithm is given.

Outline

During the ISCCP cloud algorithm intercomparison (Rossow et al., 1985) 6 fundamentally different approaches to cloud detection and characterization were compared. The merits of the individual schemes considering the boundary conditions present for the ISCCP were discussed. The schemes considered were: –visible and infrared threshold, –radiative transfer analysis (Rossow et al., 1985), –hybrid bi–spectral threshold (Minnis and Harrison, 1984a,b,c), asymmetric Gaussian analysis (Simmer et al, 1982) and –dynamic cluster analysis (Desbois et al. 1982). The study focussed on the retrieval of clear sky surface properties. All algorithms , which work well for some cloud types or climate regions, do poorly for other situations. A new algorithm was proposed which is based mainly on the following assumptions: temporal variability of the surface is low with respect to reflectivity and temperature in comparison to clouds; clouds are colder and reflect more sunlight than the underlying surface (WMO, 1988).

Step 1: Obtaining clear sky radiances

Spatial infrared test: For a processing area (100x100 km^2 over land and 300x300 km^2 over ocean) each measurement that is colder than the warmest measurement minus the threshold is flagged cloudy. The other measurements are flagged undecided.

Temporal infrared test: If the temperature of an area is the same as one day before or one day after the measurement the area is flagged clear. If the spatial test result is undecided and the temporal tests result is clear the area is flagged clear.

Temporal visual test: From a period of 5 days the minimum reflectance is obtained. Each measurement of higher reflectance, plus the threshold, is flagged cloudy.

Step 2: Spatial and temporal averaging

From the clear measurements spatial and temporal statistics are calculated. Short term extremes are compared to long term extremes. This evaluation is a check on the 'clearness' of the measurements. From the set of checked clear pixels the surface temperature and reflectivity for a 5–day period for the processing area is derived.

Step 3: Cloud flagging

The surface properties which are derived in step 2 are used as measure for all measurements in the processing area over the 5–days period. If an area is colder than the surface temperature by more than the threshold the area is flagged cloudy. And if an area has a higher reflectivity than the derived surface reflectivity by more than the threshold the area is flagged cloudy.

These are the main principles. However, there are more tests performed and statistical parameters derived. The strength of the algorithm is its applicability for each location on earth,

at each time of day and each season, because all tests are comparisons between the current local measurement and measurements nearby in space and time.

Meteorological phenomena and remote sensing

A number of studies confirm that the assumptions of the ISCCP cloud detection algorithm with respect to the temporal and spatial variability of clouds are in general correct (Seze et al., 1987,1991a,b). However, some meteorological phenomena oppose general statements. We will evaluate four meteorological phenomena separately. The cases should be considered examples of possible artifacts illustrating the difficulty of making general valid statements about cloud detection from space.

Cloud top temperatures which are equal to clear area surface temperatures

During the night the surface cools down. The surface is colder in clear areas where the atmospheric radiation is low than in cloudy areas where clouds prevent the surface to cool down. In case of an inversion the temperature difference between cloudy areas and clear areas may be negligible or positive.

Cold front

In case of a cold front passage the day to day difference in surface temperature can be 10 degrees or more. In step 1 this will cause clear cold areas to be flagged cloudy. Moreover, it is not possible to define the surface temperature for a 5–day period.

Persistent cloudiness

In order to calculate cloud amounts in step 3, the surface properties must be derived. However, there are regions which are cloudy for months (at a specific local time). Measurements of surface properties are scarce and thus the derived surface properties are not very reliable.

High spatial variability

There are areas with high spatial variability of surface temperature and reflectivity: mountains, lakes, coastal areas. For these areas the surface properties are not well defined. In the algorithm overestimation of cloudiness is prevented by increasing the thresholds. However, this decreases the sensitivity of the algorithm to cloud types with low contrast like low broken cloud fields and high semi–transparent cirrus clouds.

Areas with high spatial variability also introduce a typical remote sensing problem. One implicit assumption in the ISCCP algorithm is that the satellite measures exactly the same area each day. In practise this is not true. The pixel position is defined with a limited accuracy, which is typically half the pixel size. It is possible that a pixel is homogeneous one day, but partly filled with a mountain, lake or ocean on the next, changing the temperature or/and reflectivity. The algorithm can flagg a clear area cloudy or visa versa.

Literature study

Recently there have been comparisons between ISCCP derived cloudiness and other data sets: AVHRR (Weare, 1992); Nimbus–7 and Meteor (Mohkov et al., 1993); synoptical observations and Landsat (Rossow et al., 1993b,c). The most evident conclusion to all these studies is that a direct comparison cannot be made accurately. The observed cloud amount depends on the instrument: the spectral bands, the field of view and the viewing angle with respect to the target

area and the sun. For example in the ISCCP algorithm a measured area is clear or overcast. This implies that partly cloudy areas are classified fully cloudy, which results in an overestimate of cloud amount. On the other hand the ISCCP algorithm is not very sensitive to low broken clouds or high semi–transparent cirrus, because they generate to little contrast with clear areas. This causes an underestimate of cloud amount. This effect is most evident if a comparison to very high resolution satellite measurements like Landsat is made (Rossow et al., 1993c). For large closed cloud fields the derived cloud amounts correlate well. Studies reveal that the ISCCP algorithm has a balance between the mechanisms that cause underestimates and overestimates (Wielicki et al., 1992).

The study by Rossow et al. (1993a,b,c) are the most complete so far. In general the conclusions of the other studies do not contradict these results. ISCCP cloud amounts are compared to synoptic observations and Landsat measurements. The algorithm performance decreases with: a) increasing variability of the surface albedo and temperature, b) decreasing contrast between clouds and surface and c) decreasing temporal variability of the cloud fields. In terms of geographical areas: The derived cloud fraction is too low about 10% over land and 10–20% in polar regions. The derived cloud fractions are approximately correct over ocean.Over land the spatial variability of the surface is higher than over ocean, which makes cloud detection more difficult. The polar regions have high surface albedo (snow and ice) and low surface temperature, which reduces the contrast between cloud and surface.

The algorithm is hampered by areas of persistent cloud fields and storm tracks. As stated above persistent cloudiness and cold fronts decrease the accuracy of the derived surface properties. Two cloud types are missed frequently: low broken cloud fields and high semi– transparent cirrus clouds. Both cause little contrast in albedo and brightness temperature and are hard to identify especially over cold bright surfaces (polar regions) or highly variable land surfaces.

During the night the ISCCP algorithm has to rely on the infrared channel only. This causes underestimate of cloud amounts of low level clouds. A comparison of the day/night difference in cloud amount can not be made reliably. In general cloud amounts derived from both channels and infrared only differ 10% during daytime.

Cloud properties, cloud top temperature, cloud top pressure and cloud optical thickness are hardly validated, because reliable reference measurements are scarcely available.

Cloud climatology

The cloud climatology over the period 1982–1988 shows a global mean annual cloud cover of 63%, which is on the higher end of the range of values which are reported in literature. Over ocean there is 23% more cloudiness than over land. The month to month variation in global cloudiness is smaller than 1%. In a period of 4 years the mean global cloud amount varies about 4%.However, the local monthly mean cloudiness varies from year to year as much as 8%.

Polar regions show the least and the tropics the most seasonal variations in cloud amount . When interpreting these values we must keep in mind that the cloudiness over land is probably underestimated by 10% which decreases the difference in cloud amount over ocean and over land (Rossow et al, 1993c).

Outlook

The KNMI cloud detection system (section 2) will provide high resolution cloud characteristics over a small area. The combination of ground based and satellite measurements makes it possible to obtain accurate values of cloud height, cloud temperature and cloud optical thickness, which will be compared with the results of the ISCCP algorithm. This will enable us to validate the ISCCP cloud products.

Conclusions

The ISCCP cloud amounts provide the most reliable global cloud climatology so far and should be used by climate modelers to asses the reliability of their model with respect to clouds. Comparison with other data sets, however, revealed that ISCCP monthly mean cloud amounts are too low over land by 10% and over polar regions by 10–20%. Daytime products are more reliable than nighttime. Cloud properties, cloud top temperature, cloud top pressure and cloud optical thickness are hardly validated, because reliable reference measurements are scarcely available. Results from the KNMI Cloud Detection System may serve as a truth set.

5. ERBE

AIM

The aim of this study is to evaluate the Earth Radiation Budget Experiment (ERBE) data set for use in climate modeling. The data processing scheme, which is used to convert raw radiometer counts into monthly mean values of outgoing radiation at the top of the atmosphere, is evaluated. Topics for research were:

a) the distribution of errors over the globe and the time of day,
b) how to use ERBE data most reliably, and
c) study the possibility of improving the data processing scheme in order to upgrade the data set.

A full description of the study are given in Feijt (1991), an outline is given below.

INTRODUCTION

The Earth Radiation Budget consists of three parts: the incident solar radiation, the outgoing longwave and outgoing shortwave radiation (OSW). The net radiation budget varies widely with location and time. Temporal variations in the budget are present on an annual, but also on a diurnal scale.

The Earth Radiation Budget Experiment (ERBE) is designed to measure the Earth radiation budget on a global scale (Barkstrom et al., 1986). The objectives of ERBE are to determine:

1) The monthly average radiation budget on regional and global scales.
2) The equator to pole gradient of the radiation budget.
3) The average diurnal variation of the radiation budget on a regional and monthly scale.

ERBE consists of three satellites carrying an ERB instrument package, which consists of a scanning (Kopia, 1986) and nonscanning (Luther, 1986) radiometer for the detection of solar incoming radiation, reflected (solar) outgoing shortwave radiation (0.2–5 μm) and emitted outgoing longwave radiation (5–50 μm). The scanning radiometer has a narrow field of view and scans along the earth surface perpendicular to the direction of movement of the satellite. The focus of this report will be on the scanning radiometer because the data processing scheme is relatively simple and yield better results then the nonscanning radiometer.

The ERBE data represent the energy budget of our climate. The ERBE data set includes the spatial distribution of monthly mean regional outgoing longwave radiation, the energy loss of the Earth due to thermal radiation. The difference between the outgoing shortwave radiation and the insolation yields is the radiation energy absorbed at each region. Combination of the data of outgoing longwave radiation and absorbed solar energy yields values for the energy transport by atmospheric and oceanic currents. The ERBE data are used to test Global Climate Models (Smith, 1984) and radiation models (Rossow et al., 1990). ERBE data was used to calculate the influence of clouds on the Earth radiation budget (Ramanathan et al., 1989; Harrison et al., 1990). They calculated the monthly global cloud radiative forcing to vary between −14 and −21 W/m2.

INSTRUMENTATION

The scanning radiometers are on board of the Earth Radiation Budget Satellite (ERBS) and NOAA–9 and –10. The footprint of the ERBS scanner is 31*47 km^2, for the NOAA scanners 44*65 km^2. The difference is due to the different orbit of the ERBS, which circles at 600 km altitude in comparison with the NOAA satellites which circle at 850 km. All involved satellites are polar orbitters. NOAA–9 and 10 are sun–synchronous and have a fixed equator crossing time of 7.30 and 19.30 LT respectively. ERBS is a precessing satellite with a period of 37 days. Only during part this period a location is monitored. The time of overpass is different each day, so ERBS can monitor the diurnal variation. The scanning instruments were operational from:

* ERBS November 1984 to February 1990
* NOAA–9 February 1985 to January 1987
* NOAA–10 October 1986 to May 1989

DATA PROCESSING

Raw radiometer counts from the scanner are converted to monthly mean total outgoing radiation at the top of the atmosphere (Smith, 1986). The steps in a simplified scheme for scanner data processing are:

1) conversion from counts to radiance
2) conversion from radiance to total outgoing radiation
3) spatial and temporal averaging (TSA) to obtain the regional monthly mean.

Step 1 is not straightforward, because the response of the radiometer is not the same for all wavelengths. Therefore the detector is sensitive to the spectral signature of the incoming radiation, which is not known.

nr.	surfacetype	cloud amount
1	ocean	clear
2	land	clear
3	snow/ice	clear
4	desert	clear
5	coastal	clear
6	ocean	partly cloudy
7	ocean	mostly cloudy
8	land	partly cloudy
9	land	mostly cloudy
10	coastal	partly cloudy
11	coastal	mostly cloudy
12	overcast	overcast

Table. 1: The 12 ERBE scene types.

Step 2 is the conversion of the measured radiance at one viewing and azimuth angle to a value for all upwelling radiation, the total outgoing radiation. The contribution of the measured direction to the total outgoing radiation is the the anisotropy factor., which is not known. The spectral signature and anisotropy function is different for each individual scene and depend on surface features, cloud distribution and viewing geometry. Therefore 12 types scenes were defined of which the radiation characteristics were derived from Nimbus–7 measurements, (Suttles, 1988, 1989). There are four types of surface: ocean, land, snow/ice and desert, and four types of cloud cover: clear (0–5%), partly cloudy (5 – 50%), mostly cloudy (50–95%) and overcast (95–100%). The scene types are listed in table 1.Coastal is defined: more than 33% water and more than 33% land. For each measurement the surface type is obtained from a geophysics data base. The amount of cloud cover is determined using the Maximum Likelihood Estimate (MLE) (Wielicki and Green, 1989). The maximum likelihood estimate method is a standard approach to satellite image analysis. It is used to assign cloud classes to areas. The

ERBE MLE is used to assign a scene type to each measurement.

After scene identification the counts are converted to radiances using the scene type specific spectral response function. Radiances are converted to outgoing radiation using scene type specific anisotropy functions. Time and space averaging (TSA) yields the regional monthly mean value.

ERROR SOURCES

In this paragraph the error sources are evaluated. Estimates of the magnitude of the errors are given in the next section.

There are four types of error sources: sampling errors, scene identification errors, errors in the scene type specific radiation characteristics and time/space averaging errors.

Sampling errors include: field of view nonuniformity, the area is a mixture of snow, land and lakes. The area the field of view covers depends on the scan angle. At nadir the ellipse is 44*64 km^2. At the sides the ellipse is elongated to 250 km.

The cloud amount estimate through the MLE method is not reliable. Diekmann and Smith (1989) investigated the misclassification problem by intercomparing the results from the MLE method with results using Advanced Very High Resolution Radiometer (AVHRR) data. The intercomparison shows that there is a tendency for underestimating cloud amount over ocean at high cloud amounts, for example partly cloudy instead of mostly cloudy. On the other hand clear ocean scenes are often misclassified (compared to AVHRR scenes) as partly cloudy.

In many places in the ERBE data-processing sequence the scene type specific radiation characteristics (N7-data base) are used. The anisotropy factor for shortwave (SW) radiation can range from 0.5 to more than 2 depending on viewing angle and cloud cover. It is well known that measurements of broken cloud fields are hard to interpret. Theoretical studies by Davies (1984) and an analysis of satellite measurements by Coakley and Davies(1986) have shown that the 3-dimensional structure of broken clouds strongly influences the reflected radiances, e.g. by reflections from the sides of the clouds. This implies that misinterpretation of the amount of cloud cover will lead to significant errors in the obtained values for outgoing radiation.
Within each scene type the radiative properties vary widely. The dispersion of SW models for each scene type averaged over all viewing angles and azimuths ranges from 18 to 40%. The calculation of one value of outgoing radiation may yield a erroneous result if the signature of the scene is significantly different from the mean. On the average the deviations should cancel out if the cloud climate has not changed since the period the Nimbus-7 measured the radiation properties of the scene types from 1979 to 1985. The dispersion is worst for partly and mostly cloudy scenes.

The Time and Space Averaging (TSA) uses inter- and extrapolation of measurements in order

to fill all hour boxes for the regional monthly data matrix. The errors resulting from time sampling depend on the interval between measurements and therefore on the number of satellites involved (Brooks et al., 1986). Brooks and Minnis (1984) simulated data retrieval using the TSA to obtain insight in the relation between sample rate (number of satellites involved) and the bias and rms errors. The standard deviation (due to time/space averaging) for monthly mean net radiation values for a three satellite system is 3 W/m^2, however, 7 and 11 W/m^2 for a two satellite system of ERBS plus NOAA-10 or NOAA-9 respectively.

ERROR ESTIMATES

From the first results, obtained in April 1985, the ERBE science team has derived estimates for the standard deviations in the measurements (Barkstrom et al., 1989). These are: instantaneous radiances: LW 1%, SW 2-3%. Outgoing radiation: LW 5 W/m^2, SW 15 W/m^2. Monthly averaged scanner derived outgoing radiation: LW 5 W/m^2, SW 5 W/m^2. Global annual average: NET 5 W/m^2.

Harrison et al. (1990) has given an overview of the error estimates reported so far. Largest contributions to the errors originate from misclassification of particular scene types and sampling deficiencies. Misclassification may result in biases in the outgoing radiation for a specific scene type. Sampling errors occur when not all variations in meteorology and optical properties are accounted for. ERBE identifies snow-covered scenes as either clear or overcast. The cloud amount classification algorithm over snow is considered unreliable.

Large errors due to mis-classification of clear-sky over land situations are found. Evidence from a study by Hartmann and Doelling (1991) suggests that the nighttime, clear-sky longwave flux over oceans may be overestimated by about 6-7 W/m^2.

One of the main design considerations for ERBE was to obtain data from a multiple satellite system in order to reduce errors in time averaging. Unfortunately the three satellite system only lasted 3 months. The NOAA-9 scanner barely outlived its design lifetime of two years and the launch of NOAA-10 was delayed for half a year.

The loss of NOAA-9 scanner also has implications for the derived diurnal cycle. Cheruy et al. (1991a,b) derived outgoing longwave radiation from the geo-stationary Meteosat satellite. Cheruy states that ERBE is not able to measure the amplitude nor phase of the OLR diurnal cycle correctly due to the reduced measurement rate. The monthly mean outgoing radiation is correct though.

CAN ERBE BE UPGRADED?

The basis of the ERBE data-processing scheme is the N7-database. The largest errors are due to the large dispersion in anisotropy functions and cloud amount misclassification. To reduce the errors a new reference data set should be developed. To this end a new set of scenes should be defined and characterized using the Nimbus-7 measurements. However, it seems hardly possible to define scene types with considerably lower dispersion.

To reduce the chance of misclassification the Maximum Likelihood Estimate method should be improved. One could argue that there are more sophisticated ways to retrieve values for cloud amount. However, the MLE was designed not to obtain the correct amount of clouds, but to link real-time scanner measurements to reference values, namely the N7-database. The MLE only calculates the probability that a measurement relates to a scene type from which many characteristics are known. Introducing another cloud amount retrieval method will not improve the link between measurement values and reference values and so will not solve the misidentification problem.

CONCLUSIONS

When using monthly mean scanner values one should be aware that specific regions show considerable biased values. The standard deviations in the regional monthly mean values are of the order of 5 W/m^2. Instantaneous scanner values should be used with caution, because the accuracy is highly dependent on the viewing geometry and scene type. The accuracy can be increased considerably by choosing viewing geometries with corresponding anisotropy factors near unity. Errors due to scene misidentification and anisotropy factor errors will then be relatively small.

The nonscanner measurements are still to be reviewed, so they are not available yet. Probably the errors in the nonscanner measurements will exceed those of the scanner measurements due to the more complicated data-processing scheme and the dependence on scanner data. When the scanner instrument has stopped operation, another error is introduced.

6. RACMO

INTRODUCTION

A Regional Atmospheric Climate Model (RACMO) has been developed at KNMI in collaboration with the Danish Meteorological Institute (DMI) (Christensen and Van Meijgaard, 1992). The model combines the physical parametrization package of the General Circulation or Climate Model (ECHAM3–GCM) used at the Max Planck Institute (MPI) for Meteorology in Hamburg (Roeckner et al., 1992), and the dynamics package of the High Resolution Limited Area Model. HIRLAM is used in several European countries for purposes of operational weather forecasting (Gustafsson, 1993).

In numerical weather and climate models the various physical processes in the atmosphere are accounted for by physical parametrization schemes. In particular in climate studies the quality of physical parametrization schemes is of crucial importance. Since late 1991 a research effort at KNMI is directed to establish an environment for intercomparison and validation of atmospheric models, with a special focus on physical parametrizations. The aim is to improve the understanding of the behavior of the various physical parametrizations and their role in mutual interactions. This is especially relevant for the modeling of cloud–radiative processes, including the impact on the hydrological cycle. For this purpose the ECHAM3 physics package linked to the HIRLAM model serves as a RACMO baseline model. This model in itself is already quite valuable since it combines a treatment of the HIRLAM dynamics with the physics package of an up–to–date climate model.

MODEL ENVIRONMENT

The first version of RACMO (1992) was designed for a CONVEX–system only as this system was available at the three institutes of interest, i.e. DMI in Kopenhagen, MPI in Hamburg, and KNMI in De Bilt. A major goal was to make a fully portable code including the system shell scripts needed to manage a model run. This property was already present in the HIRLAM–system. The ECHAM3 model, however, had a entirely different structure which did not support the feature of portability. In the construction of the RACMO, therefore, a large effort was needed in making the physics package as flexible as possible. To achieve this requirement the entire package was coded in a so–called *plug compatible* or *pluggable* form, implying that all variables containing physical information are communicated with the physics manager interface through a parameter dummy–list.

MODEL DESCRIPTION

The RACMO computes the time evolution of the state of the atmosphere. This is done for a designated region with limited horizontal dimensions. The model–prognostic variables are the multi–level fields of horizontal windcomponents, temperature, specific humidity, specific liquid water, and the single–level surface pressure field. Vertical velocity is determined from the continuity equation, while the model–layer pressure values are given by integrating the hydrostatic equation upward starting at the surface pressure. Furthermore, to maintain the correct boundary conditions at the bottom of the model, prognostic equations for the

temperature and moisture of the surface and soil–layers over land are solved. Also snow pack temperature, snow thickness, and sea–ice temperature are determined from prognostic equations. The sea–surface temperature, however, is prescribed by climatic or observed values.

To describe the vertical variation of the prognostic variables the atmosphere is divided into discrete layers. In ECHAM3 and in RACMO the number of layers is 19. A terrain following vertical coordinate is employed which is a hybrid form of the absolute pressure and the pressure relative to the surface pressure. The discretization is non–equidistant with increased resolution near the earth's surface in order to describe the mixing of heat, moisture and momentum in the planetary boundary layer. In ECHAM3 and RACMO three layers have been added to the stratosphere to account for relatively slow radiative processes.

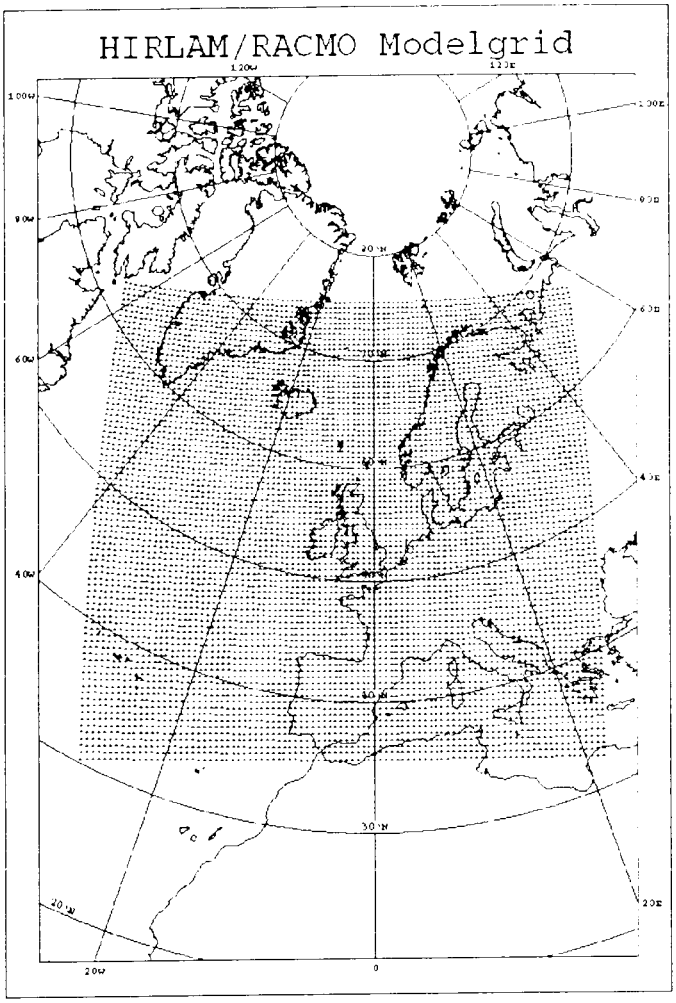

fig. 6: The HIRLAM/RACMO modelgrid

RACMO and HIRLAM run on a similar type of horizontal grid. Figure 6 shows the grid that is presently used at KNMI. It is a shifted and/or rotated latitude–longitude grid with a resolution of 0.5^0 in both directions. At mid–latitudes this corresponds to grid–point distances of about 55~km. Since the model is non–global, the grid is confined by lateral boundaries where the values of the prognostic variables are taken from a global circulation model, e.g. the ECMWF–model (European Centre for Medium Range Weather Forecast) used for numerical weather predictions or the ECHAM climate model. This procedure is called *nesting*. Boundary fields from GCM's are supplied with 6–hour intervals. At intermediate timesteps linear interpolation is employed. The RACMO is initialized from either a ECMWF–analysis or a HIRLAM–analysis.

Evidently, the apparent advantage of using a limited area model is that it offers the possibility to carry out a high–resolution study of the climatic variables in an area of interest, without being bothered with the full complexity of a global run. The size of this area however can not be chosen arbitrarily small since it should be prevented that the lateral boundary conditions dictated by the coarser GCM directly affect the interior of the regional model. In recent years this issue has received significant attention (Dickinson et al., 1989; Sass and Christensen, 1994).

DYNAMICS

As mentioned in the introduction the dynamics in RACMO is taken from the HIRLAM system. The dynamics include the transport of the prognostic variables by the mean flow as computed by the model. To solve for horizontal advection a centered second order finite difference scheme is used. Liquid water, however, which is not present in HIRLAM, is advected according to an upstream differential scheme. Time evolution is done with a leapfrog time stepping scheme with a time step size of typically 5 minutes. The procedure is semi-implicit, and in order to mix odd and even steps Asselin time-filtering is applied. Numerical horizontal diffusion is applied according to a linear fourth-order scheme; q-diffusion uses height-dependent coefficients.

PHYSICS

The physics package in the RACMO is taken entirely from the ECHAM3 global climate model. As this model is developed solely for climate studies it must be up-to-date with respect to the most recent developments in physical parameterizations. HIRLAM, however, is an operational weather forecast system with the requirement that model output is available in due time. This implies that the model, and in particular the model physics, is restricted seriously in terms of CPU-time at the expense of the level of sophistication of the physics package. As a consequence RACMO exceeds HIRLAM by about 50% in both CPU- and memory-demands.

In the standard ECHAM3 physics package the following physical processes can be distinguished:

* radiation
* vertical diffusion
* gravitational wave drag
* shallow and deep convection
* large scale condensation
* surface and soil processes

A detailed description of the ECHAM3-model including a comprehensive list of references can be found in Roeckner et al., 1992

The *pluggable* form of the RACMO-physics makes it rather straightforward to exchange a specific physics module by an alternative parametrization. As such the extended Morcrette scheme for radiative transfer (Morcrette, 1991) and a non-local formulation of the vertical mixing process (Holtslag and Boville, 1993) have been included in the RACMO.

SINGLE-COLUMN MODEL

In the past two years a single-column version of the RACMO has been formulated as well. With the single-column model the effect of modified physics parameterizations or alternative formulations can be studied extensively prior to the implementation in the three-dimensional model. Apart from the ECHAM3 physics package it contains a master routine which replaces the initialization and time-integration of the three-dimensional model. Only the physical processes for one designated point (referred to as receptor point)

are calculated. For such a point a lot of model output is made available in order to obtain a complete overview of the evolution of the modeled processes.
To be able to reproduce realistic events with a single–colum model the effects related to dynamical processes like lateral advection must be prescribed. This can be done either with observations, though this is often quite inaccurate, or with the results of a 3D–model. To support the latter option a separate module has been added to the RACMO in order to archive the dynamic tendencies of prognostic variables at *a priori* selected receptor points.

APPLICATIONS

Once a day a 36–hour forecast run is made with the RACMO based on the 00–UT HIRLAM–analysis. Boundary relaxation is done with prognosed fields obtained from ECMWF–model results. The intention of performing forecast–runs is twofold: to study the model characteristics and to save advection terms for one receptor point, in casu a grid–point near De Bilt. This is done for purposes of future research with the single–column model in combination with the observations from the CDS network.

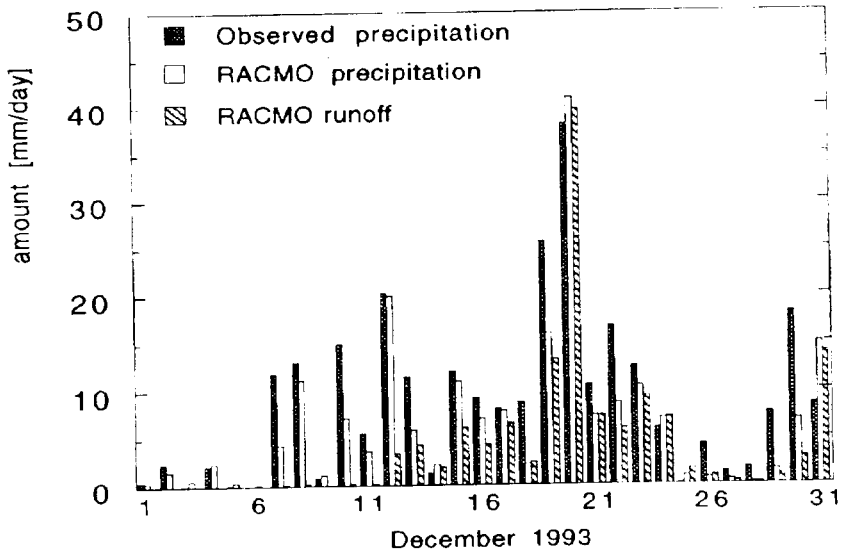

fig. 7: Precipitation and runoff in the Mease basin for December 1993.

As an application the predictions for precipitation over the Belgian Ardennes and Northern–France during December 1993 were evaluated and compared to results obtained with the HIRLAM, the UKMO–model (United Kingdom MetOffice) and the ECMWF–model (Van Meijgaard, 1994). This particular month was chosen in view of the extensive flooding of the river Meuse in the Dutch province Limburg just before Christmas 1993.

For the same month a run with the RACMO in verification–mode was carried out as well. In such a mode the model makes a long run lasting one week up till several months or a

year, and is initialized only once. In the period of interest, the lateral boundaries are prescribed by the ECMWF–analyses, so–called *perfect boundaries*. The ability of the model to generate a realistic evolution of the atmospheric state can be verified against either the ECMWF–analyses or direct observations. In this example the model run was started on 1 December 1993. Figure 7 shows that the RACMO is very well capable in reproducing the characteristics of the precipitation time series over the forementioned areas, though the total observed amount was underestimated by about 30 %. The shown runoff quantity may serve as an input parameter in a model for the river discharge. From this study it may be concluded that the RACMO is able to maintain a realistic atmospheric state for a prolonged period of integration.

FUTURE PLANS

In terms of model description and infrastructure the following extensions are planned in the near future:

* to include ECHAM4 physics in RACMO
* to make RACMO suitable for CRAY–system specific environment
* to select a limited area of interest without any restrictions on its location on earth

The latter is part of a recently initiated project directed to a study with the RACMO of the massbalance and radiative properties of the Antarctics. In another project the RACMO will be part of a model validation study with observations taken during the Azores Stratocumulus Experiment (ASTEX). Finally, observations provided by the cloud–radiation component of the Tropospheric Energy Budget Experiment (Stammes et al., 1994) will be used to study standard and alternative formulations of physical parametrizations related to cloud–radiative processes. This will primarily be done within the framework of the single–column model with lateral advections prescribed.

7. RADIATIVE TRANSFER PARAMETERIZATIONS FOR CLIMATE MODELING PURPOSES

INTRODUCTION

Radiation transfer is known to be a process of the utmost importance for the climatic equilibrium of the Earth's atmosphere system. The only significant source of energy for this system is the shortwave radiation originating from the sun. Radiation in the longwave part of the spectrum, which is emitted to space, must be considered as the ultimate sink of energy. All scenario's of climate changes are directly or indirectly linked to radiative feedback mechanisms (i.e. CO_2 enhanced greenhouse effect, ice–albedo feedback, cloud feedbacks etc.). Some studies (e.g. Fels and Kaplan, 1975; Ramanathan et al., 1983) have pointed out that simulated model climates are very sensitive to the parameterization of radiation transfer. Consequently, due to the fact that water vapor and clouds have the most pronounced impact on the radiation balance in our climate system, knowledge on the hydrological cycle is essential (Cess et al., 1989).

It will be clear that an accurate parameterization of the radiative processes in the atmosphere and at the Earth's surface is essential for climate modeling. Systematic errors in for instance the computation of the planetary radiation budget should be avoided if we want to prevent spurious indications of climate trends.

Agreement between calculated and observed radiation fields at the top of the atmosphere is a necessary condition, but does not ensure that either the surface radiation budgets or the atmospheric heating rates are modeled adequately, while these quantities influence the model dynamics predominantly. A correct representation of the radiative processes is important, not only for climate models, but also for numerical weather prediction models (forecasting over the medium and long–range as well as assimilating meteorological observations). This can be concluded from studies by Albrecht et al. (1986) and by Betts and Ridgway (1988), in which they demonstrated that there is a strong relationship between the surface fluxes in the tropics, linking the radiative and convective processes, and the large scale subsidence in the subtropics in the maintenance of the Hadley circulation. In that respect, the interactions can occur on much smaller timescales than usually quoted for radiative response times.

THE RADIATION MODEL

The Regional Atmospheric Climate MOdel (RACMO) utilizes a radiation scheme, which is based on the ECMWF code (Morcrette, 1991). The code contains 2 spectral regions in the shortwave region: visual (0.25–0.68 micron) and near infrared (0.68–4.0 micron) and 6 spectral regions in the longwave part of the spectrum (>3.5 micron). Extensions have been made for the trace gases CH_4, N_2O and 16 CFC's, HCFC's and HFC's, as in the original code only H_2O, CO_2 and O_3 (9.6 micron band) were included. Shine et al. (1995) conclude from an intercomparison study for the radiative impact of tropospheric and stratospheric ozone change scenario's, that the representation of ozone should be improved. As a result the 14 micron band of ozone has been implemented into the model. Also, Mie parameters of 11 classes of aerosols have replaced the 5 "old" aerosol types, based on the climatology of Tanre et al. (1984). These extensions and changes were necessary for climate modeling purposes. The revised version is

part of the ECHAM climate model (MPI, Hamburg).

The shortwave spectral region

The shortwave part of the radiation code originates from the scheme, developed by Fouquart and Bonnel (1980), which utilizes a two stream formulation together with a photon path distribution method.

Clear–sky computations include:

* Rayleigh scattering using a parametric expression of the Rayleigh optical thickness.
* Aerosol scattering and absorption using Mie parameters for 11 classes, based on the Global Atmospheric Data Set (GADS, Koepke et al., 1995).
* Gas absorption using the AFGL 1982 compilation of line parameters (Rothman et al., 1983) for water vapor and uniformly mixed gases in the near infrared region and ozone in both spectral regions (visible and near infrared).

For cloudy–sky computations the shortwave code employs a delta Eddington method for cloud droplet absorption and scattering. The optical thickness and single scattering albedo are determined from the liquid water path, the effective radius (function of pressure and temperature) and a preset asymmetry factor. The gas absorption is handled separately through the photon path distribution method.

The longwave spectral region

The longwave code, developed by Morcrette (1991) and extended by Van Dorland for climate modeling purposes, utilizes a broad band flux emissivity method with 6 intervals covering the spectrum for wavelengths larger than 3.5 micron. The intervals correspond to the most important features of the spectra of atmospheric constituents: the centers of the rotation and vibration–rotation bands of H_2O, the 15 micron band of CO_2, the atmospheric window, the 9.6 micron band of O_3, the 25 micron "window" region, and the wings of the vibration– rotation bands of H_2O. Temperature and pressure dependence of the absorption is computed following Morcrette (1986).

The absorption coefficients have been fitted from the GEISA 1984 compilation of spectroscopic line parameters (Husson et al., 1986 and Van Dorland and Morcrette, 1995). Overlap by other gases and aerosols is computed by multiplication of the transmission functions. The e– and p–type continuum absorption by H2O is handled separately between 8 and 28 micron. For CO_2, absorption between 8 and 20 micron, including the strong 15 micron band and the weaker bands in the atmospheric window region, is incorporated in the scheme. The strong 9.6 and weak 14 micron bands of ozone are included. For nitrous oxide, 4 spectral bands are accounted for (7.7, 8.6, 10.7 and 17.0 micron). Methane overlaps with the strong 7.7 micron vibration–rotation band. 16 species of CFC's, HCFC's and HFC's have been included in the code. Aerosols are incorporated in the code by their absorption coefficients only, while scattering in the infrared spectrum is neglected.

Cloud droplet absorption is computed from the liquid water path and effective droplet radius using an emissivity formulation. Like for aerosols, scattering by cloud droplets is neglected. The longwave fluxes for the actual atmosphere with semi-transparent, fractional and/or multi-layer clouds are derived from a linear combination of the fluxes calculated for clear-sky and (complete) overcast cloud with unity emissivity, using the random cloud overlap assumption.

FUTURE APPLICATIONS

The Global Climate Model developed at the Max Planck Institute in Hamburg (ECHAM), in which the radiation code has been incorporated, will be used for climate studies. The aims of such studies can range from the quantification of the radiative forcing due to changes of atmospheric constituents in the past and the determination of the subsequent climate effects to climate predictions for the 21th century due to expected increase of trace gas concentrations and changes in aerosol loadings.

For studies with the Regional Atmospheric Climate MOdel (RACMO) emphasis is put on the validation of the physical package, which is similar to the incorporated routines in the ECHAM model. As a consequence, RACMO will also be used for the development of new parameterizations (i.e. cloud modules). Part of the validation can be done within the context of the Tropospheric Energy Budget EXperiment (TEBEX), supported by the Dutch National Research Program. By virtue of this experiment, the boundary layer, cloud and radiation modules are essentially involved in the validation.

Another testing environment is the KNMI Radiative-Convective Model (KRCM), in which the extended radiation scheme is the central part. The main purpose is the determination of the specific features and climate sensitivity to changes of atmospheric constituents, like trace gases and aerosols. For instance, a first estimate of the greenhouse effects of aircraft emissions within the flight corridor has been obtained by computing the radiative forcing of all the constituents, which are directly emitted or indirectly formed (Fortuin et al., 1994). Also, the KRCM can be used as an off- line model for the determination of the radiative forcing from fields computed with tracer transport/chemistry models, i.e. the computation of the zonally averaged forcing due to simulated changes of tropospheric ozone since pre-industrial times (Lelieveld and Van Dorland, 1995). Finally, the KRCM is suitable for performing case studies of local forcing mechanisms, as was done for the radiative impact of the Antarctic ozone hole deepening over a 20-year period (Van Dorland and Fortuin, 1994).

Conclusively, the radiation code is being used in the assessment of climatic effects due to anthropogenic emissions in European and national frameworks for science and policy making.

8. DAK

INTRODUCTION

The Doubling–Adding radiative transfer model, called DAK (Doubling–Adding KNMI), has been developed at KNMI in the past years to simulate shortwave spectra and vertical profiles of irradiance, radiance and polarization in the Earth's atmosphere. The computer code of the DAK model consists of a monochromatic radiative transfer kernel, which solves the multiple scattering problem, and a shell of atmospheric information based on actual atmospheric composition observations or climatology.

There are at least three applications of DAK: 1. Simulation of radiances and polarization at the top–of–the–atmosphere (TOA) to interpret satellite measurements at solar wavelengths. Relevant satellite instruments are: GOME, SCIAMACHY, POLDER, AVHRR, Meteosat, and ATSR–2. Example of an application: retrieval of cloud optical thickness from satellite measurements of reflectivity in the visible wavelength range. 2. Simulation of spectral irradiances, radiances and polarization inside the atmosphere to interpret ground based or airborne radiation measurements. Example of an application: interpretation of UV irradiances measured at KNMI. 3. Calculation of spectral irradiances (radiative fluxes) at TOA and inside the atmosphere to test radiation parameterizations used in climate models. Example of an application: test of a broad–band parameterization of irradiances for the UV–visible wavelength range.

The main characteristics of the DAK model are: a) monochromatic; this means that a spectrum is calculated line–by–line, b) the atmosphere is modeled by a stack of homogeneous, plane–parallel layers, c) multiple scattering is treated exactly (as many scattering directions are taken into account as needed for a specified accuracy), d) polarization can be fully included (four Stokes parameters), e) only solar radiation is incident, f) the following scattering and absorption processes are included: molecular scattering, gas absorption (only weak bands, e.g. those of O_3), aerosol scattering and absorption, cloud particle scattering and absorption, and surface reflection and absorption. Not yet included in the present version of the model are: strong line absorptions by e.g. H_2O, O_2, CO_2 and thermal emission (internal sources).

Compared to almost all other radiative transfer models, the DAK model is unique in its inclusion of polarization. This is important to interpret satellite measurements of polarization (which will be performed by GOME, SCIAMACHY, and POLDER), but also to accurately simulate atmospheric radiances, especially in the UV. Recently, DAK results have been successfully compared with UV irradiance measurements (Kuik et al., 1994). The DAK computer code is presently being extended with spectral surface albedos and line absorptions, and its execution speed is being enhanced.

DETAILS OF THE MODEL

The core of the model is the doubling–adding algorithm. The approach of solving the problem of multiple scattering in a vertically inhomogeneous atmosphere by means of doubling and adding layers has been conceived by Van de Hulst (1980). The starting point is a very thin layer of which the reflection and transmission properties can be calculated analytically from single and double scattering. This layer is repeatedly doubled, taking into account internal reflections at the interface, until a specified optical thickness is reached and the reflection and transmission

properties of this homogeneous layer are found. By adding different layers, taking again into account the reflections at the interface, the reflection and transmission properties of a vertically inhomogeneous atmosphere can be found. The extension of the doubling–adding method to polarization has been described by De Haan et al. (1987) and the extension to the internal radiation field by Stammes et al. (1989). The doubling–adding method has been tested extensively and compared with other radiative transfer methods, and was found to be accurate and fast.

In the doubling–adding algorithm three parameters are needed for every layer of a multi–layer atmosphere: (i) the (extinction) optical thickness, (ii) the single scattering albedo, and (iii) the scattering matrix (also called phase matrix). The latter parameter describes the angular scattering and polarization properties of a volume–element of the layer. For spherical aerosol and cloud particles a Mie program is used to calculate off–line the scattering matrix. The atmospheric shell of the program calculates these three parameters for every layer, given the following input files: pressure, temperature, and trace gas mixing ratio profiles, taken from radiosonde data or climatology (McClatchey et al., 1972); background aerosol concentration profile; the LOWTRAN7 aerosol climatology is included (Kneizys et al., 1988) and special aerosol or cloud particle optical parameters. At the moment shortwave spectral absorption by O_3, NO_2, and SO_2 is included in the model. Therefore, the model can only accurately calculate the atmospheric radiation between about 250 and 700 nm, i.e. the UV and visible range, and at specific atmospheric windows in the near–IR. A recent description of the model, with the formulae used, is given by Stammes (1994).

Various types of output from DAK are possible: 1) Spectra of irradiance, radiance, and polarization at TOA or the surface for a certain wavelength range. 2) Vertical profiles of irradiances and heating rate for a specific wavelength. 3) Dependence of reflected and transmitted (ir)radiances of a cloud on its optical thickness, varying from 0 to 512, per wavelength.

SOME COMPUTATIONAL RESULTS

In this section some results of DAK are shown to demonstrate the various output types and applications.

Radiance and polarization spectra

Figure 8 shows the UV spectrum of nadir reflectivity* and degree of linear polarization at the TOA for three atmospheric cases:

(1) clear case: atmosphere with only air and ozone, and a dark surface (albedo 0.05);

(2) aerosol case: same as clear case but with aerosol added;

(3) bright surface case: same as aerosol case but with a bright surface (albedo 0.5).

The solar zenith angle is 75 deg. The bright surface case may be regarded as a simple model of homogeneous low cloud. The spectral structure in reflectivity and polarization is due to ozone absorption.

* note: Reflectivity is defined as π times the radiance divided by the solar irradiance at TOA.

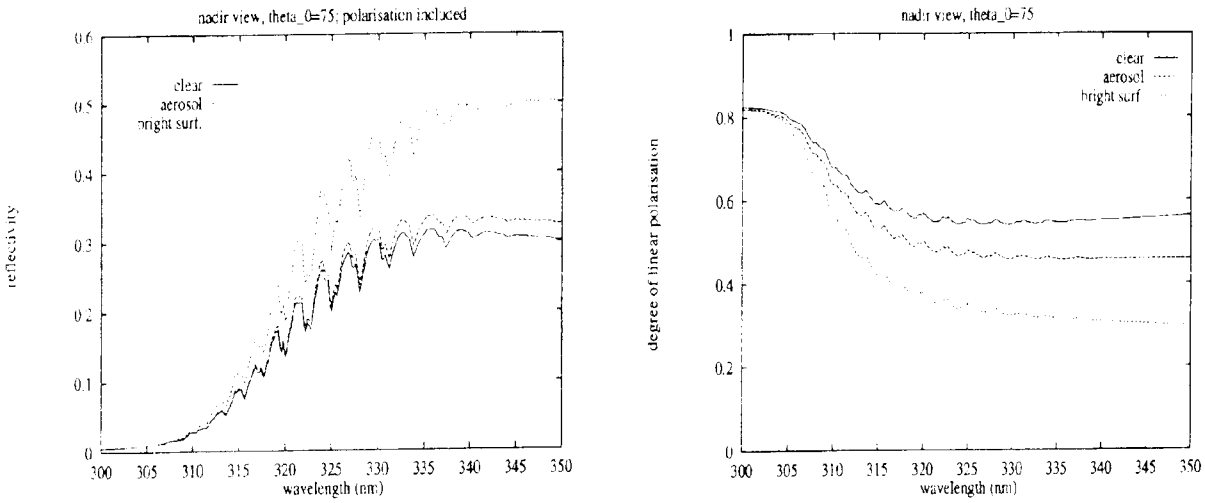

Figure 8: Calculated UV spectrum of reflectivity (a) and degree of linear polarization (b) in the nadir direction at TOA for three cases: clear atmosphere, aerosol atmosphere, and atmosphere with bright surface (see text). The solar zenith angle, theta_0, is 75 deg.

Vertical profile of downward irradiances

Figure 9 shows the profile of total downward irradiance (normalized to the solar irradiance at TOA) in a clear and a cloudy atmosphere at 500 nm. The cloud is situated between 1 and 2 km and has an optical thickness of 10. Three solar directions are given: the cosine of the solar zenith angle is 0.2, 0.6 and 1.0.

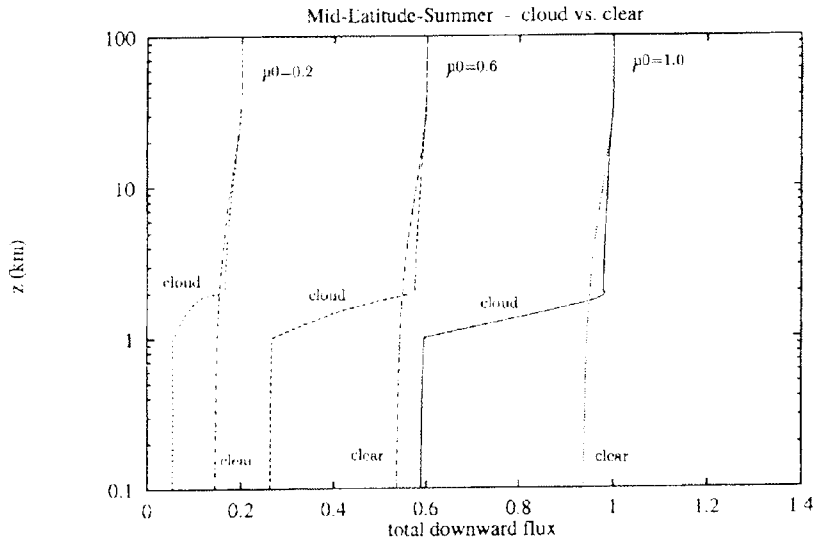

Figure 9: Calculated vertical profile of the downward flux (or irradiance) at 500 nm, normalized to the incident flux perpendicular to the solar direction, in a clear and a cloudy atmosphere, for three solar directions: mu_0=cos theta_0=0.2, 0.6 and 1.

Cloud reflectivity as a function of its optical thickness

Figure 10 shows the reflectivity of a cloudy atmosphere at 600 nm when the cloud optical thickness is varied from 0 to 512. Various solar zenith angles are used.

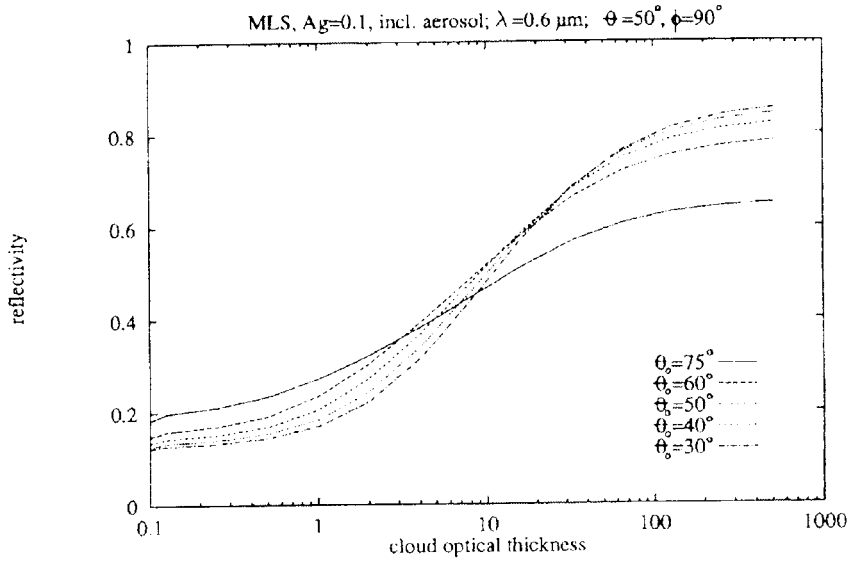

Figure 10: Calculated reflectivity at TOA at 600 nm as a function of cloud optical thickness. The chosen geometry pertains to a specific Meteosat view of the Netherlands: satellite zenith angle is 50 deg, relative azimuth sun–satellite is 90 deg, and the solar zenith angle, theta_0, is varying.

REFERENCES

Section 1

Cess R.D. et al., 1989: Interpretation of cloud–climate feedback as produced by 14 atmospheric General Circulation Models, *Science*, 245, 513–516.

Ramanathan, V., R. D. Cess, E. F. Harrison, P. Minnis, B. R. Barkstrom, E. Ahmad, D.Hartmann, 1989: Cloud– radiative forcing and climate: Results from the Earth Radiation Budget Experiment, *Science*, 243, *57–63.*

Section 2

Feijt A.J, 1994.: Integration of ground based observations in the retrieval of cloud characteristics from Meteosat data, In Proc. of the 10–th Meteosat Data Users' Meeting, Eumetsat, Darmstadt (in press).

Gesell G., 1989: An algorithm for snow and ice detection using AVHRR data: An extension to the APOLLO software package, *Int. J. Remote Sens.*, 10, 897–905.

Gesell G. et al., 1993: SHARK–APOLLO quantitative satellite data analysis based on ESRIN/SHARP and DLR/APOLLO, In Proc. of the 6–th AVHRR European Data Users' Meeting, 583–587, Eumetsat, Darmstadt.

Kneizys F.X. et al., 1988: Users' guide to Lowtran–7, AFGL–TR–88–0177, Environmental Research Paper No. 1010, Air Force Geophysics Laboratory, Hanscom AFB(MA), .

Kriebel K.T., R.W. Saunders and G. Gesell, 1989: Optical properties of clouds derived from fully cloudy AVHRR pixels, *Beitr. Phys. Atmosph,* 62, 165–171.

Monna W.A.A, 1994: On the use of wind profilers in meteorology, *Ann. Geophys.*, 12, 482–486.

Rossow W.B. and L.C. Garder, 1993: Cloud detection using satellite measurements of infrared and visible radiances for ISCCP, *J. Climate*, 6, 2341–2369.

Rossow et al., 1988 (Revised 1991),: The International Satellite Cloud Climatology Project (ISCCP) – Documentation of cloud data, WMO/TD–266, Geneva.

Saunders R. W., 1986: An automated scheme for the removal of cloud contamination from AVHRR radiances over western Europe. *Int. J. Remote Sensing,* 7, 867–886.

Saunders R.W. and K.T. Kriebel, 1988: An improved method for detecting clear sky and cloudy radiances from AVHRR data, *Int. J. Remote Sensing,* 9, 123–150.

Saunders R.W., 1988: Cloud–top temperature–height: a high resolution imagery product from AVHRR data, *Met. Mag.*, 117, 211–212.

Stammes, P., A.J. Feijt, A.C.A.P. van Lammeren, and G.J. Prangsma, 1994: TEBEX observations of clouds and radiation – potential and limitations; KNMI Technical Report 162, KNMI, De Bilt.

Stammes P.: Influence of clouds on radiative flux profiles and polarization, in *IRS '92: Current problems in atmospheric radiation*, Eds. S. Keevallik and O. Karner, 129–132, A. Deepak, Hampton, VA 1993.

Section 3

Stephens G.L., 1978: Radiation profiles in extended water clouds. II: parametrization schemes, *J. Atmos. Sci.*, 35, 2123 – 2132.

Rossow W.B. et al., 1988 (Revised 1991),: The International Satellite Cloud Climatology Project (ISCCP) – Documentation of cloud data, WMO/TD–266, Geneva.

Section 4

Desbois M., G. Seze and G. Szejwach, 1982: Automatic classification of clouds on Meteosat imagery: Application to high–level clouds, *J. Appl. Meteorol.*, 21, 401–412.

Minnis P. and E.F. Harrison, 1984a: Diurnal variability of regional cloud and clear sky radiative parameters derived from GOES data. Part I: Analysis method, *J. Climate Appl. Meteor.*, 23, 993–1011.

Minnis P. and E.F. Harrison, 1984b: Diurnal variability of regional cloud and clear sky radiative parameters derived from GOES data. Part II: November 1978 cloud distributions , *J. Climate Appl. Meteor.*, 23, 1012–1031.

Minnis P. and E.F. Harrison, 1984c: Diurnal variability of regional cloud and clear sky radiative parameters derived from GOES data. Part III: November 1978 radiative parameters. *J. Climate Appl. Meteor.*, 23, 1032–1051.

Mokhov I.I. and M.E. Schlesinger, 1993: Analysis of global cloudiness – 1. Comparison of Meteor, Nimbus 7 and ISCCP satellite data, *J. Geophys. Res.*, 98, D7, 12 849–12 868.

Ramanathan V. et al.,1989, Cloud radiative forcing and climate: Results from the earth radiation budget experiment, *Science*, 243, 57–63.

Rossow W.B. and L.C. Garder: Cloud detection using satellite measurements of infrared and visible radiances for ISCCP, *J. Climate*, 6, 2341–2369, 1993.

Rossow W.B. and L.C. Garder, 1993: Validation of ISCCP cloud detections, *J. Climate*, 6, 2370–2393,

Rossow W.B., A.W. Walker and L.C. Garder, 1993: Comparison of ISCCP and other cloud amounts, *J. Climate*, 6, 2394–2418.

Rossow W.B. and R.A. Schiffer, 1991: ISCCP cloud data products, *Bull. Am. Meteorol. Soc.*, 72, 2–20.

Rossow W.B., F. Mosher, E. Kinsella, A. Arking, M. Desbois, E. Harrison, P. Minnis, E. Ruprecht, G. Seze, C. Simmer and E. Smith, 1985: ISCCP cloud algorithm intercomparison, *J. Climate Appl. Meteor.*, 24, 877–903.

Seze G. and W.B. Rossow, 1991a: Time–cumulated visible and infrared histograms used as description of surface and cloud variations, *Int. J. Remote Sensing*, 12, 877–920.

Seze G. and W.B. Rossow, 1991b: Effects of satellite data resolution on measuring the space/time variations of surfaces and clouds, *Int. J. Remote Sensing*, 12, 921–952.

Simmer C., E. Raschke and E. Ruprecht, 1982: A method for determination of cloud properties from two–dimensional histograms. *Ann. Meteor*, 18, 130–132.

Weare B.C., 1992: A comparison of ISCCP C1 cloud amounts with those derived from high resolution AVHRR images, *Int. J. Rem. Sensing*, 13, 1965–1980.

Wielicki B.A. and L. Parker, 1992: On the determination of cloud cover from satellite sensors: The effect of sensor spatial resolution. *J. Geophys. Res.*, 97, 12 799–12 823.

World Meteorological Organization, 1978: Report of the JOC study conference on parametrization of extended cloudiness and radiation for climate models, Oxford, 27 September – 4 October 1978, WCP–6, WMO, Geneva.

World Climate Program, 1982: The International Satellite Cloud Climatology Project (ISCCP) – Preliminary Implementation Plan (Rev.1). WCP–35, WMO, Geneva.

World Climate Program, 1986: The International Satellite Cloud Climatology Project (ISCCP) – Research plan and validation strategy Plan , WMO/TD–88, Geneva.

World Climate Program, 1988 (Revised 1991),: The International Satellite Cloud Climatology Project (ISCCP) – Documentation of cloud data, WMO/TD–266, Geneva.

Section 5

Barkstrom, B. R. and G. L. Smith, 1986: The Earth Radiation Budget Experiment: Science and implementation, *Rev. Geophys*, 24, 379–390.

Barkstrom. B. R., E. Harrison, G. Smith, R. Green, J. Kibler, R. Cess and the ERBE Science team, 1989: Earth Radiation Budget Experiment (ERBE) Archival and April 1985 Results, *Bull. Am. Meteorol. Soc.*, 70, 1254–1262.

Brooks, D. R. and P. Minnis, 1984: Simulations of the Earth's monthly regional radiation balance derived from satellite measurements, *J. Clim. Appl. Meteorol.*, 23, 392–403.

Brooks, D. R., E. F. Harrison, P. Minnis, J. T. Suttles and R. S. Kandel, 1986: Development of algorithms for understanding the temporal and spatial variability of the Earth radiation balance, *Rev Geophys.*, 24, 422– 438.

Cheruy F., R.S. Kandel and J.P. Duvel, 1991a: Outgoing longwave radiation and its diurnal variation from combined ERBE and Meteosat observations: 1. Estimating OLR from Meteosat data, *J. Geophys. Res.*, 96, 22 611–22 622.

Cheruy F., R.S. Kandel and J.P. Duvel, 1991b: Outgoing longwave radiation and its diurnal variation from combined ERBE and Meteosat observations: 2. Using Meteosat data to determine the longwave diurnal cycle, *J. Geophys. Res.*, 96, 22 623–22 630.

Coakley, J. A. and R. Davies, 1986: The effect of cloud sides on reflected solar radiation as deduced from satellite observations, *J. Atmos. Sci.*, 43, 1025–1035.

Davies, R., 1984: Reflected solar radiances from broken cloud scenes and the interpretation of scanner measurements, *J. Geophys. Res.*, 89, 1259–1266.

Diekmann, F. J. and G. L. Smith, 1989: Investigation of scene identification algorithms for radiation budget measurements, *J. Geophys. Res.*, 94, 3395–3412.

Feijt A.J., 1992: The earth radiation budget: overview of data–processing and error sources, KNMI TR–146, KNMI, De Bilt.

Harrison E. F., P. Minnis, B. R. Barkstrom, V. Ramanathan, R. D. Cess and G. G. Gibson, 1990: Seasonal variation of cloud radiative forcing derived from the Earth Radiation Budget Experiment, *J. Geophys. Res*, 95, 18,687–18,703.

Hartmann, D. L., and D. Doelling, 1991: On the net radiative effectiveness of clouds, *J. Geophys. Res.* 96, 869–891.

Kopia, L. P., 1986: Earth Radiation Budget Experiment scanner instrument, *Rev. Geophys*, 24, 400–406.

Luther, M. R., J. E. Cooper and G. R. Taylor, 1986: The Earth Radiation Budget Experiment

non–scanner instrument, *Rev. Geophys*, 24, 391–399.
Ramanathan, V., R. D. Cess, E. F. Harrison, P. Minnis, B. R. Barkstrom, E. Ahmad, D. Hartmann, 1989: Cloud– radiative forcing and climate: Results from the Earth Radiation Budget Experiment, *Science*, 243, 57–63.
Rossow, W. B., Y. Zang and A. A. Lacis, 1990.: Calculations of atmospheric radiative flux profiles, In 7th Am. Met. Soc. Conf. Atmos. Radiat., Boston, Mass., 81–86
Smith, G. L., R. N. Green, E. Raschke, L. M. Avis, J. T. Suttles, B. A. Wielicki and R. Davies, 1986: Inversion methods for satellite studies of the Earth's radiation budget: Development of algorithms for the ERBE mission, *Rev. Geophys*, 24, 407–421.
Suttles, J. T., R. N. Green, P. Minnnis, G. L. Smith, W. F. Staylor, B. A. Wielicki, I. J. Walker, D. F. Walker, D. F. Young, V. R. Taylor and L. L. Stowe, 1988: Angular radiation models for the Earth– atmosphere system. Vol I: Shortwave radiation. NASA Ref. Publ. RP–1184, 147pp.
Suttles, J. T., G. L. Smith, B. A. Wielicki, I. J. Walker, V. R. Taylor and L. L. Stowe, 1989: Angular radiation models for the Earth–atmosphere system. Vol II: Longwave radiation. NASA Ref. Publ. RP–1184, 87pp.
Taylor, V. R. and L. L. Stowe, 1984: Reflectance characteristics of uniform Earth and cloud surfaces derived from Nimbus–7 ERB. *J. Geophys. Res.*, 89, 4987–4996.
Wielicki, B. A. and R. N. Green, 1989: Cloud identification for ERBE radiative flux retrieval. *J. Appl. Meteorol.*, 28, 1133–1146.

Section 6

Christensen, J. H. en E. van Meijgaard, 1992: On the construction of a regional atmospheric climate model; KNMI Technical report 147 (De Bilt), and DMI Technical report 92–14 (Copenhagen).
Dickinson, R. E., R. M. Errico, F. Giorgi, and G. T. Bates, 1989: A Regional Climate Model for the Western United States; *Climatic Change*, 15, 383–422.
Gustafsson, N., 1993: HIRLAM 2 Final Report; HIRLAM Technical Report No. 9.
Holtslag, A.A.M., and B.A. Boville, 1993: Local versus Nonlocal Boundary–Layer Diffusion in a Global Climate Model; *J. of Climate*, 6, 1825–1842.
Meijgaard, E. van, 1994: Evaluatie van neerslagprognoses van numerieke modellen voor de Belgische Ardennen in december 1993; KNMI Technical report 169, KNMI, De Bilt.
Morcrette, J.–J., 1991: Radiation and cloud radiative properties in the ECMWF forecasting system; *J. Geophys. Res.*, 96, D5, 9121–9132.
Roeckner, E. et al., 1992: Simulation of the present–day climate with the ECHAM–model: Impact of model physics and resolution; Max–Planck Institute fur Meteorologie, Report No.93.
Sass, B.H., and J.H. Christensen, 1994: A simple framework for testing the quality of atmospheric limited area models; HIRLAM Technical Report No. 15, SMHI, Norkopping
Stammes, P., A.J. Feijt, A.C.A.P. van Lammeren, and G.J. Prangsma, 1994: TEBEX observations of clouds and radiation – potential and limitations; KNMI Technical Report 162, KNMI, De Bilt.

Section 7

Albrecht, B.A., V. Ramanathan, and B.A. Boville, 1986: The effects of cumulus moisture transport on the simulation of climate with a general circulation model, *J.Atmos.Sci.*, 43, 2443–2462.

Betts, A.K., and W. Ridgway, 1988: Coupling of the radiative, convective and surface fluxes over the Equatorial Pacific, *J.Atmos.Sci.*, 45, 522–536.

Cess R.D. et al., 1989: Interpretation of cloud–climate feedback as produced by 14 atmospheric General Circulation Models, *Science*, 245, 513–516.

Fels, S.B., and L.D. Kaplan, 1975: A test of the role of longwave radiation transfer in a general circulation model, *J.Atmos.Sci.*, 32, 779–789.

Fortuin, J.P.F., R. van Dorland, W.M.F. Wauben, and H. Kelder, 1994: Greenhouse effects of aircraft emissions as calculated by a radiative transfer model, *Ann.Geophys*, (in press).

Fouquart, Y., and B. Bonnel, 1980: Computations of solar heating of the earth's atmosphere: A new parameterization, *Beitr. Phys. Atmosph.*, 53, 35–62.

Husson, N., A. Chedin, and N.A. Scott, 1986: The GEISA spectroscopic line parameters bank in 1984, *Ann.Geophys.*, 4, A2, 185–190.

Morcrette, J.–J., L. Smith, and Y. Fouquart, 1986: Pressure and temperature dependence of the absorption in longwave radiation parameterizations, *Beitr. Phys. Atmosph.*, 59, 455–469.

Morcrette, J.–J., 1991: 'Radiation and cloud radiative properties in the ECMWF forecasting system', *J.Geophys.Res.*, 96, D5, 9121–9132.

Lelieveld, J., and R. van Dorland, 1995: Ozone chemistry changes in the troposphere and consequent radiative forcing of climate, *Atmospheric Ozone as a Climate Gas*, W.–C. Wang and I.S.A. Isaksen (eds.), NATO ARW Series, Springer (in press).

Ramanathan, V., E.J. Pitcher, R.C. Malone, and M.L. Blackmon, 1983: The response of a spectral general circulation model to refinements in radiative processes, *J.Atmos.Sci.*, 40, 605–630.

Rothman, L.S., 1981: AFGL atmospheric absorption line parameters compilation: 1980 version, *Appl.Opt.*, 21, 791–795.

Shine, K.P., B.P. Briegleb, A.S. Grossman, D. Hauglustaine, H. Mao, V. Ramaswamy, M.D. Schwarzkopf, R. van Dorland, and W.C. Wang, 1995: Radiative forcing due to changes in ozone: a comparison of different codes, *Atmospheric Ozone as a Climate Gas*, W.C. Wang and I.S.A. Isaksen (eds.), NATO ARW Series, Springer (in press).

Tanre, D., J.F. Geleyn, and J. Slingo, 1984: First results of the introduction of an advanced aerosol–radiation interaction in the ECMWF low resolution global model, in *Aerosols and their climatic effects*, H.E. Gerber and A. Deepak (Eds.), A. Deepak Publishing, Hampton, Va, 133–177.

Van Dorland, R. and J.–J. Morcrette, 1995: A comparison of spectroscopic compilations using longwave radiation models, Submitted to *J. Geophys. Res.*

Van Dorland, R and J.P.F. Fortuin, 1994: Simulation of the observed stratospheric temperature trends 1967–1987 over Antarctica due to ozone hole deepening, Non CO2 Greenhouse Gases, J. van Ham et al. (eds.), Kluwer Academic Publishers, 237–245.

Section 8

de Haan, J.F., P.B. Bosma, and J.W. Hovenier, 1987: The adding method for multiple scattering calculations of polarized light, *Astron. Astrophys.*, 183, 371–391.

Kneizys F.X., et al., 1988, Users guide to LOWTRAN7, AFGL–TR–88–0177, Environmental Research Paper No. 1010, Hanscom AFB, Mass. (1988)

Kuik, F., W.M.F. Wauben, and P. Stammes, 1994: Modelling the influence of aerosol on the observed UV spectrum, Abstract for conference on Aerosols and Atmospheric Optics, Snowbird, Utah, USA, Sept. 25–30 (in press).

McClatchey, R., et al., 1972: Optical properties of the atmosphere (3rd ed.), Air Force Cambridge Research Labs., AFCRL–72–0497, 107 pp.

Stammes P., 1993: Influence of clouds on radiative flux profiles and polarization, in *IRS '92: Current problems in atmospheric radiation*, Eds. S. Keevallik and O. Karner, 129–132, A. Deepak, Hampton, VA.

Stammes, P., 1994: Errors in UV reflectivity and albedo calculations due to neglecting polarisation, Proceedings of the European Symposium on Satellite Remote Sensing, 26–30 Sept. 1994, Rome, EOS/SPIE,. 2311 (in press).

Stammes, P., J.F. de Haan, and J.W. Hovenier, 1989: The polarized internal radiation field of a planetary atmosphere, *Astron. Astrophys.*, 225, 239–259.

Stammes, P., A.J. Feijt, A.C.A.P. van Lammeren, and G.J. Prangsma, 1994: TEBEX observations of clouds and radiation – potential and limitations; KNMI Technical Report 162, KNMI, De Bilt.

van de Hulst, H.C., 1980: Multiple Light Scattering, Tables, Formulas, and Applications; Volume 1 and 2, *Academic Press, New York.*

Bijgaand treft U een overzicht aan van recentelijk in deze serie gepubliceerde titels. Een komplete lijst wordt U op verzoek toegezonden. U kunt Uw aanvraag richten aan de KNMI Bibliotheek, Postbus 201, 3730 AE De Bilt (030-206855). Hier kan men U tevens informeren over de verkrijgbaarheid en prijzen van deze publicaties.

89-01 Instability mechanisms in a barotropic atmosphere / R.J. Haarsma.

89-02 Climatological data for the North Sea based on observations by voluntary observing ships over the period 1961-1980 / C.G. Korevaar.

89-03 Verificatie van GONO golfverwachtingen en van Engelse fine-mesh winden over de periode oktober 1986 - april 1987 / R.A. van Moerkerken.

89-04 Diagnostics derivation of boundary layer parameters from the outputs of atmospheric models / A.A.M. Holtslag and R.M. van Westrhenen.

89-05 Statistical forecasts of sunshine duration / Li Zhihong and S. Kruizinga.

90-01 The effect of a doubling atmospheric CO2 on the stormtracks in the climate of a general circulation model / P.C. Siegmund.

90-02 Analysis of regional differences of forecasts with the multi-layer AMT-model in the Netherlands / E.I.F. de Bruin, Li Tao Guang and Gao Kang.

90-03 Description of the CRAU data-set : Meteosat data, radiosonde data, sea surface temperatures : comparison of Meteosat and Heimann data / S.H. Muller, H. The, W. Kohsiek and W.A.A. Monna.

90-04 A guide to the NEDWAM wave model / G. Burgers.

91-01 A parametrization of the convective atmospheric boundary layer and its application into a global climate model / A.A.M. Holtslag, B.A. Boville and C.-H. Moeng.

91-02 Turbulent exchange coefficients over a Douglas fir forest / F.C. Bosveld.

92-01 Experimental evaluation of an arrival time difference lightning positioning system / H.R.A.Wessels.

92-02 GCM control run of UK Meteorological Office compared with the real climate in the NW European winter / J.J. Beersma.

92-03 The parameterization of vertical turbulent mixing processes in a General Circulation Model of the Tropical Pacific / G. Janssen.

92-04 A scintillation experiment over a forest / W.Kohsiek.

92-05 Grondtemperaturen / P.C.T.van der Hoeven en W.N.Lablans

92-06 Automatic supression of anomalous propagation clutter for noncoherent weather radars / H.R.A. Wessels and J.H. Beekhuis.

93-01 Searching for stationary stable solutions of Euler's equation / R. Salden.

93-02 Modelling daily precipitation as a function of temperature for climatic change impact studies / A.M.G. Klein Tank and T.A. Buishand.

93-03 An analytic conceptual model of extratropical cyclones / L.C. Heijboer.

93-04 A synoptic climatology of convective weather in the Netherlands / Dong Hongnian.

93-05 Conceptual models of severe convective weather in the Netherlands / Dong Hongnian.

94-01 Seismische analyse van aardbevingen in Noord-Nederland : bijdrage aan het multidisciplinaire onderzoek naar de relatie tussen gaswinning en aardbevingen / H.W.Haak en T. de Crook.

94-02 Storm activity over the North Sea and the Netherlands in two climate models compared with observations / J.J. Beersema.

94-03 Atmospheric effects of high-flying subsonic aircraft / W. Fransen.

94-04 Cloud-radiation-hydrological interactions : measuring and modeling / A.J. Feijt, R. van Dorland, A.C.A.P. van Lammeren, E. van Meijgaard en P. Stammes.